Chinese Chemical Letters 37 (2026) 111312

Contents lists available at ScienceDirect

Chinese Chemical Letters

journal homepage: www.elsevier.com/locate/cclet

Ultrafast carbothermal shock synthesis of transition metal phosphides in air for highly efficient hydrogen evolution reaction

Tingting Liu[a,1], Ruting Lin[a,1], Yuyu Liu[a], Chen Chen[a], Qiufeng Huang[a], Yuzhi Sun[b], Shengyun Huang[b,*], Ibrahim Saana Amiinu[c], Zonghua Pu[a,*]

[a] College of Chemistry & Materials Science, Fujian Normal University, Fuzhou 350117, China
[b] Ganjiang Innovation Academy, Key Laboratory of Rare Earths, Chinese Academy of Sciences, Ganzhou 341000, China
[c] Department of Chemical Sciences, University of Limerick, Limerick, V94 T9PX, Ireland

ARTICLE INFO

Article history:
Received 29 January 2025
Revised 3 May 2025
Accepted 13 May 2025
Available online 13 May 2025

Keywords:
Ultrafast synthesis
Joule heating
Metal phosphides
Hydrogen evolution reaction
Electrocatalysis

ABSTRACT

Transition metal phosphides (TMPs) are a promising class of functional nanomaterials with significant potential for energy-related applications. However, a universal synthesis method that is both efficient and scalable remains a challenge. This study introduces an ultrafast carbothermal shock (UCS) technique as efficient method for synthesizing various TMPs, including Rh_2P, Ir_2P, Pd_5P_2, RuP and PtP_2, in just 15 s under ambient air conditions. Notably, the as synthesized Rh_2P exhibits remarkable hydrogen evolution reaction (HER) performance with low overpotentials of 13 and 70 mV to reach current densities of 10 and 100 mA/cm^2, respectively, coupled with excellent operational stability for over 20 h. This technique not only provides a universal platform for producing various metal phosphides, but also holds significant promise for advancing their applications in energy conversion and storage devices, catalysis, and biosensors.

© 2026 Published by Elsevier B.V. on behalf of Chinese Chemical Society and Institute of Materia Medica, Chinese Academy of Medical Sciences.

Reconciling the development of a sustainable, global-scale energy system concurrently with the preservation of the environment stands as one of the most critical challenges facing humanity. To date, over 80% of the energy resources supporting modern society stems from traditional fossil fuels [1–3]. Therefore, leveraging renewable energy sources, including solar, wind, marine, and hydroelectric power for electrochemical energy conversion and storage represents a promising approach to achieving energy sustainability [4–13]. In this context, clean energy storage and conversion technologies, such as hydrogen production *via* water electrolysis, various rechargeable battery systems, and fuel cells have attracted significant research interest [14–20]. Hydrogen and oxygen evolution reactions (HER and OER) are crucial electrokinetic processes for hydrogen production. Likewise, efficient oxygen reduction and evolution reactions (ORR and OER) are essential for the renewable energy sector, especially in the development of fuel cells and rechargeable batteries [21,22]. Thus, the development of catalytic system with high stability and enhanced performance for HER, OER and ORR are vital for the aforementioned energy storage and conversion systems.

In the past ten years, transition-metal phosphides (TMPs) have received considerable attention for their applications in electrocatalysis due to their outstanding physicochemical properties, including good conductivity and high catalytic activities [23,24,25–32]. However, achieving metal phosphides with stable crystal structure requires prolonged high-temperature pyrolysis ($\geq$2 h) under the inert atmosphere, which is not only time-consuming and energy-intensive but also escalates production costs. Furthermore, the extended high-temperature calcination process generates substantial CO_2 emissions. These factors contribute to increased production costs. Additionally, the toxic phosphine gas (PH_3) generated during traditional calcination can cause severe air pollution. Similarly, the dissolution-thermal method produces phosphorus-containing wastewater and organic solvent emissions, imposing supplementary economic and environmental burdens. More importantly, traditional methods often result in large particle sizes as well as agglomeration, ultimately resulting in a decline in electrochemical performance. Therefore, it is highly desirable to explore rapid synthetic approaches that enable the production of nano-sized TMP particles with enhanced surface area at lower pyrolysis temperatures and ambient air conditions. Fortunately, ultrafast carbothermal shock (UCS) synthesis allows for rapid flash heating

* Corresponding authors.
E-mail addresses: shyhuang@gia.cas.cn (S. Huang), zonghua.pu@fjnu.edu.cn (Z. Pu).
[1] This authors contributed equally to this work.

https://doi.org/10.1016/j.cclet.2025.111312
1001-8417/© 2026 Published by Elsevier B.V. on behalf of Chinese Chemical Society and Institute of Materia Medica, Chinese Academy of Medical Sciences.

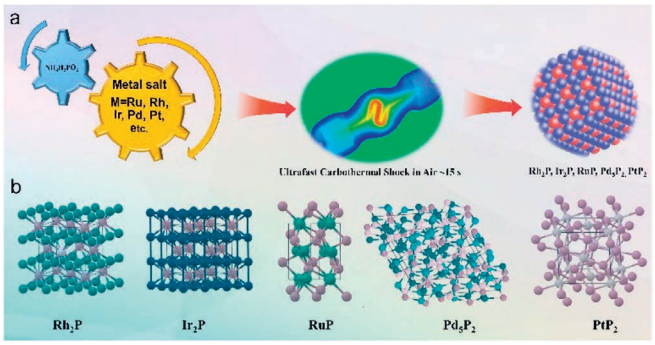


Fig. 1. (a) Schematic illustration of the synthesis process of TMPs by UCS. (b) The crystal structures of Rh_2P, Ir_2P, RuP, Pd_5P_2 and PtP_2. Purple and black-blue balls denote phosphorus and metal elements.

and cooling, with ramp rates reaching up to 10^5 K/s. This instantaneous temperature fluctuation allows reactions to complete within few seconds [33–36]. The total energy consumption is significantly reduced. On the other hand, UCS holds significant potential for continuous production, leading to lower long-term operating costs and reduced per-unit production costs as scale increases. Additionally, the low energy consumption of UCS effectively decreases carbon emissions, aligning with the principles of green manufacturing. More importantly, the optimized second-level calcination time effectively mitigates sintering and agglomeration of active components that could result from prolonged heat treatment, thereby ensuring the rapid and uniform dispersion of active atoms. This enhancement facilitates precise control over the particle size and structure of the synthesized materials.

Herein, we have successfully demonstrated an ultrafast ($\leq$15 s), energy-saving synthesis of a series of TMPs, including Rh_2P, Ir_2P, Pd_5P_2, RuP, and PtP_2, using UCS under ambient air atmosphere. Characterization results indicate that these TMPs comprise of ultrasmall nanoparticles with controllable sizes and well-defined crystalline structures, with enhanced HER activity and stability. For example, the as obtained Rh_2P exhibits platinum-like HER activity with overpotentials of 13 and 70 mV at a current density of 10 and 100 mA/cm^2 in 0.5 mol/L H_2SO_4, respectively. Such high HER activities not only surpass most reported electrocatalysts based on precious-metal phosphides, but also compared favorably to commercial Pt/C materials. Therefore, this study presents a pioneering approach to fabricating TMPs in seconds by UCS under ambient air conditions with enhanced HER performance.

The UCS synthesis process for these TMPs nanoparticles is schematically illustrated in Fig. 1a. Initially, a homogeneous mixture of metal salts and $NH_4H_2PO_2$ was prepared. Subsequently, the obtained precursor mixture was subjected to UCS under air atmosphere. Following cooling, the byproduct was extensively rinsed with deionized water to obtain the final sample. Notably, the UCS strategy enables the synthesis of various TMPs, including Rh_2P, Ir_2P, Pd_5P_2, RuP, and PtP_2 (Fig. 1b). For comparison, Rh_2P-T was also prepared *via* the calcination process in a tube furnace. As shown in Fig. S1a (Supporting information), the XRD pattern confirming the Rh_2P-T has been successfully obtained. Furthermore, TEM images show that Rh_2P-T exhibits a bulk morphology (Figs. S1b, c and S2 in Supporting information).

Powder X-ray diffraction (XRD) was used to investigate the crystallographic structure of Rh_2P, Ir_2P, Pd_5P_2, RuP, and PtP_2. As displayed in Figs. 2a, d, g, j and m, the diffraction patterns of Rh_2P, Ir_2P, Pd_5P_2, RuP, and PtP_2 match well with their standard PDF cards [37,38]. The structural features of Rh_2P, Ir_2P, Pd_5P_2, RuP, and PtP_2 are revealed by TEM (Figs. 2b, c, e, f, h, i, k, l, n and o). The TEM images in Figs. 2b and h indicate that Rh_2P and RuP are composed

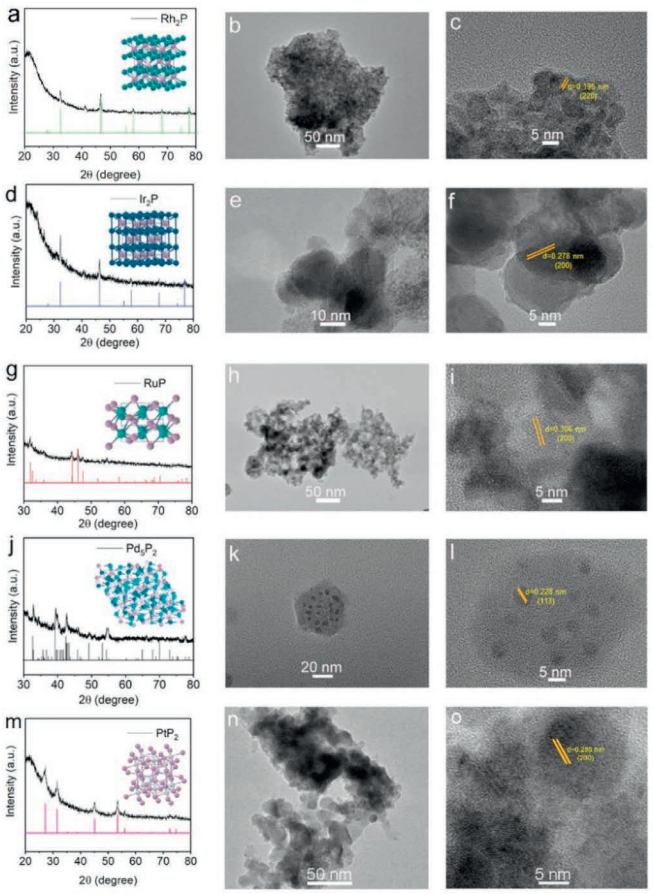


Fig. 2. (a) The XRD patterns for (a) Rh_2P, (d) Ir_2P, (g) RuP, (j) Pd_5P_2 and (m) PtP_2. TEM and HRTEM images of (b, c) Rh_2P, (e, f) Ir_2P, (h, i) RuP, (k, l) Pd_5P_2 and (n, o) PtP_2.

of small nanocrystals. The Ir_2P shows a nanosphere morphology with particle size ranges from 8 nm to 25 nm (Fig. 2e and Fig. S3 in Supporting information), while both Pd_5P_2 and PtP_2 possess a typical nanoparticles structure with particle size of ~2 and 20 nm, respectively (Figs. 2k and n, Fig. S3). Additionally, the high-resolution TEM (HRTEM) images reveal the lattice fringe spacing of Rh_2P, Ir_2P, RuP, Pd_5P_2 and PtP_2 to be 0.195, 0.278, 0.306, 0.228 and 0.285 nm, corresponding to cubic Rh_2P (220), cubic Ir_2P (200), orthorhombic RuP (200), monoclinic Pd_5P_2 (113) and cubic PtP_2 (200) crystal planes (Figs. 2c, f, i, l and o), respectively.

The energy dispersive X-ray (EDX) spectrum (Fig. S4 in Supporting information) confirms the presence of Rh and P in the Rh_2P nanoparticle, with an atomic ratio of Rh and P approaching 2:1. Furthermore, the HAADF-STEM and energy-dispersive X-ray spectroscopy (EDS) elemental mapping demonstrate homogeneous distribution of both Rh and P elements within the Rh_2P nanoparticle (Figs. 3a-d). These results demonstrate that the UCS process is energy-efficient and time-saving for fabricating a series of uniformly dispersed TMPs under an air atmosphere.

XPS was employed to further examine the elemental composition and surface chemical state of Rh_2P. The results indicate that the surface of Rh_2P is predominantly composed of C, O, Rh and P (Fig. S5 in Supporting information). The presence of elemental C and O can be assigned to the absorption of CO_2, H_2O, O_2, or slight surface oxidation of Rh_2P potentially caused by exposure to air. The XPS spectrum of the Rh 3d region exhibits two peaks at binding energies (BE) of 312.6 and 307.8 eV, corresponding to the Rh $3d_{3/2}$ and Rh $3d_{5/2}$ states of Rh_2P (Fig. 3e), respectively. In addition, the P 2p spectrum displays three distinct subpeaks at 133.9, 131.2 and

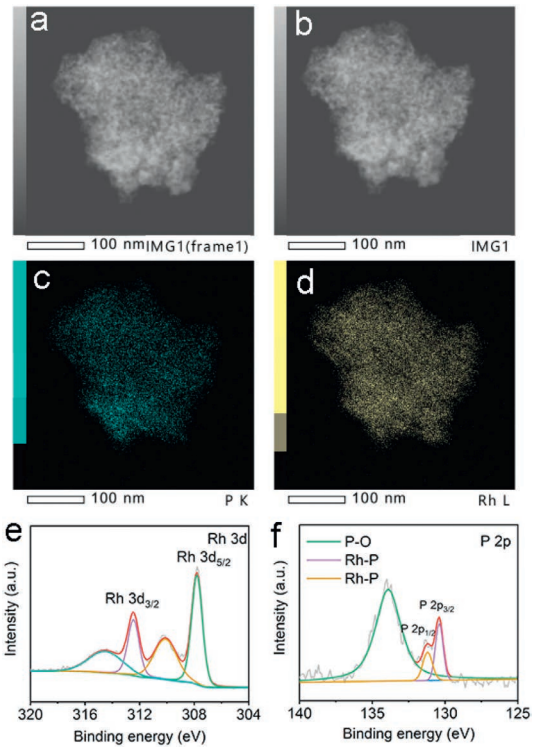


Fig. 3. (a-d) STEM images and corresponding EDS elemental mapping of Rh and P of Rh_2P. (e) Rh 3d and (f) P 2p XPS spectra of Rh_2P.

130.1 eV (Fig. 3f). The peaks observed at 131.2 and 130.1 eV can be attributed to the Rh-P bond, whereas the peak at 133.9 eV is indicative of oxidized phosphorus species. Notably, the Rh $3d_{5/2}$ peak is blue-shifted by 0.5 eV relative to the metal Rh (307.3 eV) [39], while the P $2p_{3/2}$ peak is red-shifted compared to elemental P (130.2 eV) [40]. These observations indicate the presence of a partial positive charge (δ^+) on Rh and a partial negative charge (δ^-) on P in Rh_2P, suggesting a weak electron transfer from Rh to P. The positively charged Rh atom serve as the hydride-acceptor center, while the negatively charged P atom functions as the proton-acceptor center. This dual functionality modulates the attachment and detachment of hydrogen atoms at the active sites during the subsequent HER process.

The HER activity of the obtained samples (Rh_2P, PtP_2, Ir_2P, RuP and Pd_5P_2) were examined in 0.5 mol/L H_2SO_4 electrolytes, with all potentials calibrated using an RHE as the reference scale. Before conducting the HER tests, the obtained samples were activated by performing a series of linear sweep voltammetry (LSV) scans ranging from 0 to −0.5 V *vs.* Ag/AgCl. Fig. 4a illustrates the *iR*-corrected (the internal resistance determined through EIS analysis in Fig. S6 in Supporting information) HER polarization curves of Rh_2P, PtP_2, Ir_2P, RuP and Pd_5P_2. All the samples (Rh_2P, PtP_2, Ir_2P, RuP and Pd_5P_2) obtained *via* UCS exhibits good HER catalytic activities with an onset potential close to 0 mV. Specifically, the overpotentials needed for Rh_2P, PtP_2, Ir_2P, RuP and Pd_5P_2 to achieve a cathodic current density of 10 mA/cm^2 are 13, 20, 37, 30 and 84 mV (Fig. 4b), respectively. More importantly, the catalytic activity of Rh_2P, PtP_2, Ir_2P, RuP and Pd_5P_2 is comparable to that of recently reported Rh/Pt/Ir/Ru/Pd-based TMPs synthesized by traditional methods, such as Rh_2P obtained by solution-phase reaction (14 mV@10 mA/cm^2) [41], PtP_2@NPC synthesized by high-temperature pyrolysis of mixtures of $PtCl_4$ with phytic acid under an ammonia atmosphere (320 mV@10 mA/cm^2) [42], Ir_2P-decorated Ru_2P hollow nanotubes *via* an anion/cation-exchange strategy (23.2 mV@10 mA/cm^2) [43], RuP_2@NPC obtained by thermal treatment (38 mV@10 mA/cm^2) [44], Pd_5P_2@NPGC synthesized

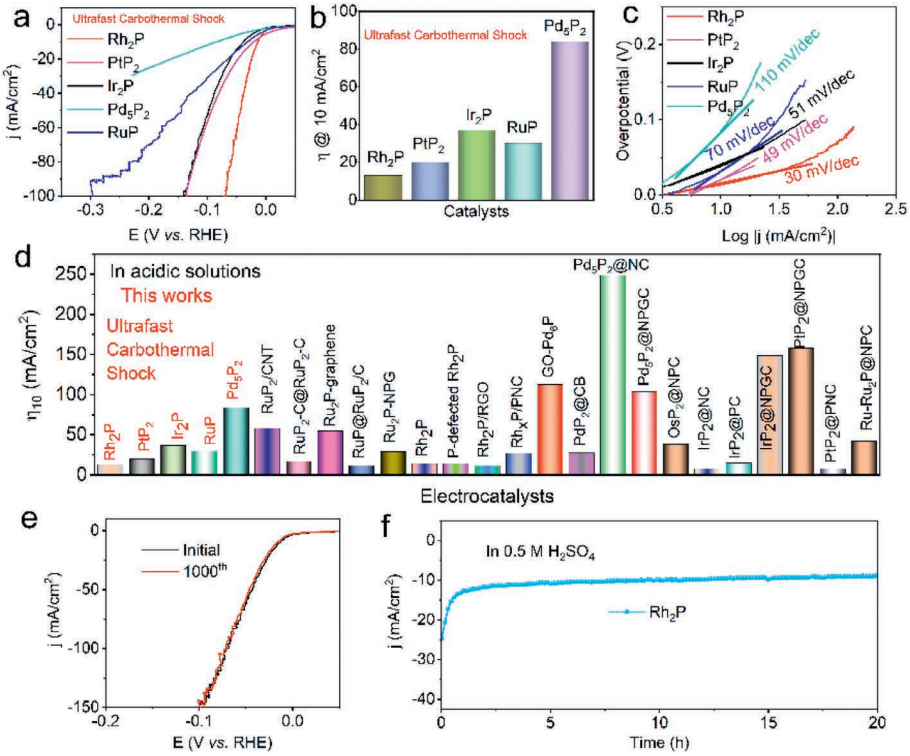


Fig. 4. (a, c) Polarization curves and corresponding Tafel plots of Rh_2P, PtP_2, Ir_2P, RuP and Pd_5P_2 in 0.5 mol/L H_2SO_4 solution. (b) Overpotentials at $j = 10$ mA/cm^2 for Rh_2P, PtP_2, Ir_2P, RuP and Pd_5P_2. (d) Overpotentials comparison for Rh_2P, PtP_2, Ir_2P, RuP and Pd_5P_2 at $j = 10$ mA/cm^2 with recently reported metal phosphides catalysts. (e) Polarization curves were recorded before and after 1000 CV potential cycles for Rh_2P. (f) Chronoamperometric test for Rh_2P in 0.5 mol/L H_2SO_4 electrolyte at constant potential for 20 h (without *iR* correction).

by traditional pyrolysis (104 mV@10 mA/cm^2) [45]. This observation suggests the superiority of UCS over conventional methods in preparing TMPs. Tafel slope is another critical parameter for assessing the HER activity of electrocatalysts. The Tafel slopes obtained from the linear region of the Tafel plots for of Rh_2P, PtP_2, Ir_2P, RuP and Pd_5P_2 are 30, 49, 51, 70 and 110 mV/dec (Fig. 4c), respectively. Similarly, these Tafel values are comparable to those reported for Pt-group TMPs synthesized using conventional ways [41–45]. Furthermore, taking Rh_2P as the research object, based on its Tafel value, it can be inferred that the hydrogen generation process of Rh_2P in acidic solutions likely follows the Volmer-Tafel mechanism, and the rate-determining step (RDS) is governed by the Tafel step: $2M\text{-}H_{ad} \rightarrow H_2 + 2M$, where M denotes the active site and H_{ad} represents the adsorbed hydrogen intermediate [46,47]. To the best of our knowledge, the high HER activity of these samples compares favorably with that of most TMPs synthesized by traditional methods (such as pyrolysis at high temperature in inert atmosphere or solution synthesis in organic solvents) reported in acidic electrolytes (Fig. 4d and Table S2 in Supporting information).

Based on the superior HER activity demonstrated by Rh_2P, we conducted an in-depth investigation into its long-term stability. Fig. 4e presents the polarization curves obtained before and after 1000 cyclic voltammetry (CV) cycles at 5 mV/s. It is worth noting that the LSV curves of Rh_2P exhibited minimal degradation even after undergoing 1000 CV potential cycles. Furthermore, the long-term stability of the Rh_2P electrocatalyst is evaluated through continuous electrolysis at a fixed overpotential of ~20 mV without iR correction. As shown in Fig. 4f, the current density of Rh_2P demonstrates negligible degradation under acidic conditions over 20 h electrolysis period, highlighting the exceptional durability of the synthesized Rh_2P. Additionally, the XRD analysis of both the fresh and post-HER Rh_2P materials (Fig. S7 in Supporting information) confirms the similarity in their crystal structures. Furthermore, inductively coupled plasma atomic emission spectroscopy (ICP-AES) analysis revealed that rhodium exhibited minimal leaching (6 %) in the electrolyte during prolonged stability testing. This limited leaching may be attributed to the partial desorption of powder electrocatalysts from the electrode surfaces due to vigorous gas evolution during the HER [48]. These resulting offering robust evidence for the retention of the Rh_2P composition and its remarkable durability under acidic media during HER.

More significantly, Rh_2P exhibits excellent HER performance under both alkaline (1.0 mol/L KOH) and neutral (1.0 mol/L PBS) conditions, requiring overpotentials of 70 and 97 mV, respectively, to achieve a current density of 10 mA/cm^2 (Fig. S8 in Supporting information). Additionally, it exhibits stable performance with operation durations of 8 h in neutral electrolytes (1.0 mol/L PBS) and 11 h in alkaline electrolytes (1.0 mol/L KOH) (Fig. S9 in Supporting information). Therefore, these comprehensive analyses demonstrate that Rh_2P is an excellent and durable catalyst material for HER in a wide pH range.

In conclusion, we have developed a facile, energy efficient, and ultrafast carbothermal shock method capable of synthesizing TMPs within 15 s under ambient air conditions. The versatility of this technique was validated through the successful synthesis of various TMPs, including Rh_2P, PtP_2, Ir_2P, Pd_5P_2, RuP and PtP_2. Electrochemical measurements confirmed that all samples exhibited high HER catalytic activity, with overpotential of 13, 20, 37, 30 and 84 mV for Rh_2P, PtP_2, Ir_2P, RuP and Pd_5P_2 required to achieve cathodic current densities of 10 mA/cm^2. This outstanding HER activity rivals that of state-of-the-art phosphides based on Pt-group metals, which are typically synthesized through conventional solid-state or solution-phase methods. Consequently, the ultrafast carbothermal shock synthesis of TMPs under ambient air conditions shows significant potential for advancing the development of TMP-based electrocatalysts for energy-related applications.

Declaration of competing interest

The authors declare that they have no known competing financial interests or personal relationships that could have appeared to influence the work reported in this paper.

CRediT authorship contribution statement

Tingting Liu: Writing – original draft, Investigation, Formal analysis, Data curation. **Ruting Lin:** Software, Investigation, Data curation. **Yuyu Liu:** Investigation, Data curation. **Chen Chen:** Investigation, Data curation. **Qiufeng Huang:** Supervision, Software. **Yuzhi Sun:** Software, Data curation. **Shengyun Huang:** Writing – review & editing, Supervision. **Ibrahim Saana Amiinu:** Writing – review & editing. **Zonghua Pu:** Writing – review & editing, Supervision, Methodology.

Acknowledgments

This work was supported by the National Natural Science Foundation of China (Nos. 22402030, 62475266), the Fujian Province Young and Middle-Aged Teacher Education Research Project (No. JZ240012), Youth Innovation Promotion Association of Chinese Academy of Sciences (No. 2023341) and Jiangxi Provincial Natural Science Foundation (No. 20232BAB204101).

Supplementary materials

Supplementary material associated with this article can be found, in the online version, at doi:10.1016/j.cclet.2025.111312.

References

[1] H.D. Graven, Proc. Natl. Acad. Sci. U. S. A. 112 (2015) 9542–9545.
[2] R.S. Haszeldine, Science 325 (2009) 1647.
[3] R.D.L. Smith, M.S. Prévot, R.D. Fagan, et al., Science 340 (2013) 60.
[4] T. Liu, C. Chen, Z. Pu, et al., Small 20 (2024) 2405399.
[5] H. Wei, D. Cui, J. Ma, et al., J. Mater. Chem. A 5 (2017) 1873–1894.
[6] Z. Lu, L. Zhao, H. Fu, et al., Nat Commun 15 (2024) 6513.
[7] D. Xu, P. Wu, H. Tan, Inf. Funct. Mater. 1 (2024) 2–25.
[8] Y. Gu, N. Nie, J. Liu, et al., EcoEnergy 1 (2023) 405–413.
[9] J. Liang, Z. Cai, Z. Li, et al., Nat. Commun. 15 (2024) 2950.
[10] J. Liang, Z. Cai, X. He, et al., Chem 10 (2024) 3067–3087.
[11] Z. Lv, S. Zhou, L. Zhao, et al., Adv. Energy Mater. 13 (2023) 2300946.
[12] Y. Yu, Z. Lv, Z. Liu, et al., Angew. Chem. Int. Ed. 63 (2024) e202402236.
[13] Y. Yu, Y. Sun, J. Han, et al., Energy Environ. Sci. 17 (2024) 5183–5190.
[14] M. Li, X. Wang, J. Meng, et al., Adv. Mater. 36 (2024) 2308628.
[15] Z. Pu, G. Zhang, A. Hassanpour, et al., Appl. Energy 283 (2021) 116376.
[16] Y. Zeng, C. Li, B. Li, et al., Nat. Catal. 6 (2023) 1215–1227.
[17] P. Mardle, B. Chen, S. Holdcroft, ACS Energy Lett. 8 (2023) 3330–3342.
[18] L. Zhao, Z. Lv, Y. Shi, et al., Energy Environ. Sci. 17 (2024) 770–779.
[19] D. Wu, H. Du, Z. Liu, et al., EcoEnergy 2 (2024) 724–735.
[20] W. Yu, Y. Zhang, Y. Qin, et al., Adv. Energy Mater. 13 (2023) 2203136.
[21] Z. Pu, T. Liu, G. Zhang, et al., Small Methods 5 (2021) 2100699.
[22] Z.W. Seh, J. Kibsgaard, C.F. Dickens, et al., Science 355 (2017) 6321.
[23] T. Liu, C. Chen, S. Liu, et al., Coord. Chem. Rev. 521 (2024) 216145.
[24] Z. Pu, T. Liu, I.S. Amiinu, et al., Adv. Funct. Mater. 30 (2020) 2004009.
[25] M. Du, D. Li, S. Liu, J. Yan, Chin. Chem. Lett. 34 (2023) 108156.
[26] Y. Shi, M. Li, Y. Yu, B. Zhang, Energy Environ. Sci. 13 (2020) 4564–4582.
[27] C. Li, D. Zhu, S. Cheng, et al., Chin. Chem. Lett. 33 (2022) 1141–1153.
[28] L. Yue, J. Liang, Z. Wu, et al., J. Mater. Chem. A 9 (2021) 11879–11907.
[29] C. Tang, R. Zhang, W. Lu, et al., Adv. Mater. 29 (2017) 1602441.
[30] Q. Liu, J. Tian, W. Cui, et al., Angew. Chem. Int. Ed. 53 (2014) 6710–6714.
[31] L. He, Z. Cai, D. Zheng, et al., J. Mater. Chem. A 12 (2024) 2680–2684.
[32] J. Tian, Q. Liu, A.M. Asiri, X. Sun, J. Am. Chem. Soc. 136 (2014) 7587–7590.
[33] Q. Dong, Y. Yao, S. Cheng, et al., Nature 605 (2022) 470–476.
[34] C.H. Choi, J. Shin, L. Eddy, et al., Nat. Chem. 16 (2024) 1831.
[35] T. Liu, Z. Chen, S. Liu, et al., Angew. Chem. Int. Ed. 64 (2025) e202414021.
[36] Z. Zhao, J. Sun, X. Li, et al., Nat. Commun. 15 (2024) 7475.
[37] Z. Pu, J. Zhao, I.S. Amiinu, et al., Energy Environ. Sci. 12 (2019) 952–957.
[38] B. Guo, J. Zhao, Y. Xu, et al., ACS Appl. Mater. Interfaces 16 (2024) 8939–8948.
[39] Y. Liu, L. Wang, H. Zhang, et al., Angew. Chem. Int. Ed. 60 (2021) 22761–22768.
[40] K. Zhou, W. Zhou, L. Yang, et al., Adv. Funct. Mater. 25 (2015) 7530–7538.
[41] F. Yang, Y. Zhao, Y. Du, et al., Adv. Energy Mater. 8 (2018) 1703489.

[42] Q. Qin, H. Jang, L. Chen, et al., ACS Appl. Mater. Interfaces 11 (2019) 16461–16473.
[43] Y. Hong, S. Jeong, J.H. Seol, et al., Adv. Energy Mater. 14 (2024) 2401426.
[44] Z. Pu, I.S. Amiinu, Z. Kou, W. Li, S. Mu, Angew. Chem. Int. Ed. 56 (2017) 11559–11564.
[45] J. Yu, X. Wu, H. Zhang, et al., ACS Appl. Energy Mater. 2 (2019) 2645–2653.
[46] G. Zhao, K. Rui, S.X. Dou, W. Sun, Adv. Funct. Mater. 28 (2018) 1803291.
[47] M.A. Habib, S. Burse, S. Lin, et al., Small 20 (2024) 2307533.
[48] C. Andronescu, S. Barwe, E. Ventosa, et al., Angew. Chem. Int. Ed. 56 (2017) 11258–11262.